



One-dimensional ZnO/Mn₃O₄ core/shell nanorod and nanotube arrays with high supercapacitive performance for electrochemical energy storage

Journal:	<i>RSC Advances</i>
Manuscript ID:	RA-COM-01-2014-000588.R1
Article Type:	Communication
Date Submitted by the Author:	19-Mar-2014
Complete List of Authors:	Liu, Zhao-Qing; Guangzhou University, School of Chemistry and Chemical Engineering Li, Nan; Guangzhou University, School of Chemistry and Chemical Engineering Wang, Ji-Yu; Guangzhou University, School of Chemistry and Chemical Engineering Su, Yuzhi; Guangzhou University, School of Chemistry & Chemical Engineering Chen, Shuang; Guangzhou institute of railway technology,

One-dimensional ZnO/Mn₃O₄ core/shell nanorod and nanotube arrays with high supercapacitive performance for electrochemical energy storage

Nan Li^a, Ji-Yu Wang^a, Zhao-Qing Liu^{a, *}, Yun-Ping Guo^a, Dong-Yao Wang^a, Yu-Zhi Su^a, Shuang Chen^b

^aSchool of Chemistry and Chemical Engineering/Guangzhou Key Laboratory for Environmentally Functional Materials and Technology, Guangzhou University, Guangzhou 510006, China

^bGuangzhou institute of railway technology, Guangzhou 510430, China

Abstract:

One-dimensional (1D) ZnO/Mn₃O₄ core/shell nanorod arrays (NRAs) and nanotube arrays (NTAs) have been controllably synthesized via a facile electrochemical deposition process and characterized by X-ray diffraction, SEM, TEM, EDS, X-ray photoelectron spectroscopy, and electrochemical experiments. To assess the properties of 1D ZnO/Mn₃O₄ core/shell nanostructures for using in supercapacitors, cyclic voltammetry and galvanostatic charging-discharging measurements were performed. Remarkably, the ZnO/Mn₃O₄ core/shell NTAs electrode is found to exhibit 2.5 times higher capacitance, better rate performance and smaller inner resistance than the ZnO/Mn₃O₄ NRAs. These findings indicate that the novel 1D architectures offer a very promising design for supercapacitors.

* Corresponding author. Tel.: +86 20 39366908; Fax: +86 20 39366908.

E-mail addresses: lzqgz@gzhu.edu.cn

1. Introduction

Owing to the depletion of fossil fuels and the escalation of environmental pollution, the development of alternative energy conversion or storage devices with high power and large energy densities is of particular significance.¹⁻⁴ In this context, supercapacitors, also called electrochemical capacitors or ultracapacitors, which can efficiently bridge the gap between high specific energy batteries and high specific power capacitors, have received considerable attention for applications in portable electronics, hybrid electrical vehicles and uninterrupted power sources. Supercapacitors have been considered the most promising storage devices because they can instantaneously provide higher power densities and higher energy densities than other energy devices, such as lithium-ion batteries and conventional dielectric capacitors.⁵⁻⁸

Recently, the use of 1D nanomaterials as the electrodes of supercapacitors has drawn great attention because they can provide short diffusion path lengths for ions, leading to high charge/discharge rates.⁹⁻¹⁰ Compared with the individual single-component nanorods, the 1D core/shell nanostructures have attracted more and more attention because they can provide a wealth of opportunities for the development of new composite materials.¹¹⁻¹² Specially, the ordered arrays of 1D core/shell nanostructures are found to improve the electrochemical performance of the electrode through fast ion diffusion, stress relaxation, and electron and mass transport. Up to now, some 1D core/shell nanostructures have been investigated for supercapacitors, such as ZnO/MoO₃ core/shell nanocable arrays,¹³ Co₃O₄

nanowire@MnO₂ ultrathin nanosheet core/shell arrays,¹⁴ and hierarchical NiCo₂O₄@MnO₂ core/shell heterostructured nanowire arrays.¹⁵ Despite intensive research efforts, constructing electrodes of supercapacitors with high specific capacitance and high electrochemical stability still remains a challenge.

The critical task for constructing a supercapacitor is exploring the electrode material, which directly determine its capacitance, delivery rate and stability. However, the traditional electrode materials, such as carbonaceous materials, RuO₂ and conducting polymers,¹⁶⁻¹⁹ do not meet the stringent requirement of supercapacitors owing to their sluggish electrode kinetics, high price or inferior electrochemical stability. To develop economical electrode materials with not only a high capacity of charge storage but also energy density, the cheap transition metal oxides as electrode materials for supercapacitors, such as nickel oxide,²⁰⁻²¹ cobalt oxide,²²⁻²³ and manganese oxide,²⁴⁻²⁶ have drawn intense interest due to their low cost and environmental benignity. Among them, the manganese oxides (MnO_x, x = 2 or 3/4) have been thorough exploited as electrode material for supercapacitors because of their outstanding structural flexibilities, high specific capacitances, rich polymorphism, cost effectiveness, low environmental toxicities, redox reversibilities, etc.²⁷⁻²⁸ Particularly, Mn₃O₄ electrode material consisted with Mn(□) and Mn(□) is a representative with the various oxidation states and would facilitate excellent pseudocapacitance.²⁹⁻³⁰ However, the poor electronic conductivity of Mn₃O₄ has hindered its further application for high-power supercapacitors. In order to solve this problem, various carbon nanomaterials have been widely utilized as supporters due to

their large surface and good electrical conductivity.³¹⁻³⁴ However, the carbon supporters possibly encounter severe corrosion in the electrochemical window of some metal oxides, and this result in a rapid degradation of the electrochemical performance. In this paper, the novel ZnO nanorod arrays supported Mn₃O₄ are investigated for supercapacitors applications. It is well known that ZnO is one of the most attractive multifunctional materials because of its specific optoelectronic and good electric conduction properties and its excellent chemical and thermal stabilities. Furthermore, to the best of our knowledge, a simple synthesis of large area ZnO/Mn₃O₄ nanotube arrays for supercapacitor application has rarely been reported yet.

In the present study, we have first demonstrated the formation of highly ordered ZnO/Mn₃O₄ core/shell NRAs and NTAs by a facile electrochemical approach and have investigated their electrochemical properties for supercapacitors. The as-prepared electrodes have the following advantages for supercapacitors: (1) The electronic conductivity has been improved due to the presence of ZnO as supports, (2) the effective surface area of the electrodes has been enhanced by using 1D ZnO NRAs, (3) the controllable shell layer of Mn₃O₄ would provide a short ion diffusion path to enable the fast and reversible faradic reaction. The 1D core/shell ZnO/Mn₃O₄ NRAs and NTAs electrodes exhibit superior capacitive performance with specific capacitance of 216.3 F/g and 441.4 F/g at a scan rate of 2 mV/s, and long cycle stability, which make this type of environmentally friendly, nontoxic core/shell nanostructures to be a perfectly promising material for supercapacitor applications.

2. Experimental

Synthesis of ZnO NRAs: All reagents used were analytical grade and were used directly without any purification. According to the previous report,³⁵ electrodeposition of ZnO NRAs precursor was performed with a HDV-7C transistor potentiostatic apparatus that connected with a conventional three-electrode cell. During cathodic electrodeposition, a glass coated with F-doped SnO₂ (FTO) with a sheet resistance of 14 Ω/□ was used as the working electrode, a graphite rod of about 4.0 cm² was used as the auxiliary electrode, and an Ag/AgCl electrode was used as the reference electrode. ZnO NRAs were synthesized in solution of 0.02 M Zn(NO₃)₂ + 0.01 M NH₄Ac + 0.01 M C₆H₁₂N₄ (HMT) by galvanostatic electrolysis with 2.0 mA/cm² for 50 min at 90 °C. The length and diameter of ZnO nanorods can be controlled by changing the electrodeposition time. After the electrodeposition, the ZnO NRAs on the FTO glass substrates was washed with deionized water and then used as the working electrode for the second electrodeposition.

Synthesis of ZnO/Mn₃O₄ core/shell NRAs and NTAs: ZnO/Mn₃O₄ core/shell NRAs and NTAs were prepared via a electrodeposition process by using the above ZnO NRAs as working electrode in an aqueous solution of 0.01 M Mn(Ac)₂ + 0.02 M NH₄Ac + 30% (CH₃)₂SO (DMSO) (30 vol % DMSO : 70 vol % H₂O) at 70 °C with current density of 0.5 mA/cm². And the heat treatment temperature was kept at 300 °C in atmosphere for 3h. The loading of Mn₃O₄ on the ZnO nanorod surface can be tunable via the optimization of different electrodeposition time.

Characterizations: The surface morphology and structure of the as-prepared samples were analyzed by using field emission scanning electron microscopy (FE-SEM, Quanta 400) and transmission electron microscopy (TEM, 300 kV, Tecnai™ G2 F30). The as-prepared samples were also characterized by energy-dispersive X-ray spectroscopy (EDX, INCA 300) to determine the deposit compositions. The structure of the samples were analyzed by powder X-ray diffraction (XRD, Bruker , D8 ADVANCE) with $K\alpha$ radiation ($\lambda = 1.5418 \text{ \AA}$). The chemical-state analysis of samples was carried out by X-ray Photoelectron Spectroscopy (XPS, ESCALab250).

Electrochemical measurements: The electrochemical properties of the as-prepared samples were investigated with cyclic voltammetry (CV), charge-discharge measurements and electrochemical impedance spectroscopy by employing a CHI 760D electrochemical workstation (Chenhua, Shanghai) in a three-compartment cell with a Pt plate counter electrode, a saturated calomel electrode (SCE) reference electrode, and a working electrode. The electrolyte was a 0.5 M aqueous solution of Na_2SO_4 .

3. Result and discussion

The $\text{ZnO}/\text{Mn}_3\text{O}_4$ core/shell nanostructures were synthesized by a two-step successive electrochemical deposition process and heat treatment method. Figure 1a-b shows the typical SEM images of the ZnO nanorods. It clearly shows that the orderly hexagonal and highly oriented ZnO nanorod arrays with smooth surface are uniformly grown onto the FTO glass substrates. The diameter and length of ZnO nanorod are 200-300 nm and $\sim 2.5 \text{ \mu m}$, respectively. The as-prepared ZnO NRAs was further

electrodeposited at 70 °C in an aqueous solution of 0.01 M $\text{Mn}(\text{Ac})_2$ + 0.02 M NH_4Ac + 30% DMSO for 15 min and then heat treatment at 300 °C in atmosphere for 3h. The SEM images of $\text{ZnO}/\text{Mn}_3\text{O}_4$ core/shell NRAs is shown in Figure 1c-d, it clearly shows that the hexagonal ZnO nanorods evolved into circular $\text{ZnO}/\text{Mn}_3\text{O}_4$ nanorods. Furthermore, the color of ZnO film changed from white to brownish, which suggests that Mn_3O_4 wraps favorably shared the surfaces of the ZnO nanorods. From the figure 1c-d, it is evident that the core of ZnO was slowly dissolved after 15 min electrodeposition time. When the electrodeposition time increased to 30 min and the heat treatment at 300 °C in atmosphere for 3h, $\text{ZnO}/\text{Mn}_3\text{O}_4$ core/shell NTAs are also successfully obtained, as shown in Figure 1e-f. To identify the phase and composition of the as-prepared samples, the X-ray diffraction (XRD) spectrum was collected and shown in Figure 2. Besides SnO_2 peaks that come from the FTO substrate, it can be clearly seen that the XRD patterns of the as-prepared samples show the hexagonal phase of wurtzite-type ZnO (space group: $P63mc$) with lattice constants $a = 3.25 \text{ \AA}$ and $c = 5.207 \text{ \AA}$, in accordance with the reported data (JCPDS: 36-1451). Mn_3O_4 peaks of (111), (220), (311), (400) and (511) are also observed in the XRD pattern, which show a cubic structure (JCPDS: 13-0162, $a = b = c = 8.42 \text{ \AA}$). The result reveals the as-prepared samples are composed of $\text{ZnO}/\text{Mn}_3\text{O}_4$. Furthermore, the intensity of Mn_3O_4 peaks in $\text{ZnO}/\text{Mn}_3\text{O}_4$ NTAs significantly improved, indicating the thickness of Mn_3O_4 is increased through the longer electrochemical reaction time.

The detailed crystal structure and composition of the product were further characterized using transmission electron microscopy (TEM). Figure 3a-b shows

TEM images of the as-prepared ZnO/Mn₃O₄ core/shell nanorod, and that the thickness of Mn₃O₄ shell is homogeneous. The high-resolution TEM (HRTEM) image in Figure 3c displays a lattice spacing of 0.24 nm, corresponding to be (222) plane of Mn₃O₄. Additionally, the corresponding EDS pattern of ZnO/Mn₃O₄ core/shell nanorod is shown in Figure 3d, besides the Cu and Mg signals coming from the substrate of measuring device, the remaining signals all come from Mn, Zn and O in sample, which also further confirms the core/shell nanorod is ZnO/Mn₃O₄. Figure 4a is the TEM image of the ZnO/Mn₃O₄ core/shell nanotube, which clearly shows the tube diameter is about 260 nm. The cross-section TEM image of ZnO/Mn₃O₄ core/shell nanotube is shown in figure 4b, which shows the wall thickness is about 100-200 nm. Figure 4c is the HRTEM image of the ZnO/Mn₃O₄ core/shell nanotube, and an enlarge HRTEM image and corresponding selected area electron diffraction (SAED) pattern of the ZnO nanorod recorded from the white square are presented in Figure 4d. Such core/shell nanostructures exhibit a slightly larger ZnO (0001) plane spacing of 0.52 nm, and the SAED pattern from the as-prepared samples shows that the core of ZnO is of the wurtzite structure. The shell of Mn₃O₄ appears to be polycrystalline with a cubic structure, as shown in Figure 4e-f. In addition, the surface-grown Mn₃O₄ is clearly visible along with lattice fringes formed from the (222), (311) and (220) planes, which exhibit 0.24 nm, 0.25 nm and 0.29 nm spacing as measured from the images, respectively. In order to further elucidate microscopic structure, the TEM-EDX (energy dispersive X-ray) elemental full and line mapping techniques were applied to an individual ZnO/Mn₃O₄ nanotube. As shown in Figure 4g-i, it can

be seen that Mn, Zn, and O are distributed as like nanotube. Based on the results above, it is believed that the as-prepared samples are ZnO/ Mn₃O₄ NRAs and NTAs.

X-ray photoelectron spectroscopy (XPS) was also conducted to characterize the surface composition of the ZnO/ Mn₃O₄ NRAs and NTAs, as indicated in Figure 5. Figure 5a compares the XPS survey spectra of the ZnO/ Mn₃O₄ NRAs and NTAs. In comparison to ZnO/ Mn₃O₄ NRAs, the XPS survey spectrum of ZnO/ Mn₃O₄ NTAs exhibits the stronger Mn 2P peaks (marked by blue dashed rectangle). Figure 5b shows the core level Zn 2p XPS spectrum of ZnO/ Mn₃O₄ NTAs. Two obvious peaks located at 1022 and 1045 eV are observed, which are consistent with the values reported for Zn²⁺.³⁵ It can be observed that the Mn 2p peak consists of two main spin-orbital lines. The Mn 2p_{3/2} peak is centered at 641.1 eV and the Mn 2p_{1/2} peak at 654.0 eV, with a splitting of 11.9 eV, which is in good harmony with literature values.³⁶⁻³⁷ The Mn 2p spectrum was convoluted as two pairs of doublets by Gaussian curve fitting: 641.6 and 642.9 eV, 653.8 and 655.1 eV, corresponding to Mn³⁺ 2p_{3/2} and Mn²⁺ 2p_{3/2}, Mn³⁺ 2p_{1/2} and Mn²⁺ 2p_{1/2}, respectively. An asymmetric two-band structure is observed in the O 1s spectrum. It is resolved into two components, corresponding to the binding energies of 530.2 and 532.2 eV, respectively. The fitting low energy peak centered at 530.2 eV is characteristic of the lattice oxygen of ZnO and Mn₃O₄. The high binding energy peak located at 532.2 eV is normally physisorbed, chemisorbed or dissociated oxygen or hydroxyl species on the surface of samples.³⁸⁻³⁹ On the basis of the XPS results, it is believed that the core/shell nanostructures consist of ZnO and Mn₃O₄.

To verify the applicability of ZnO/Mn₃O₄ core/shell nanostructures as supercapacitor electrodes, their electrochemical properties were investigated in terms of their prolonged cycling performance. Cyclic voltammetry (CV) and galvanostatic charge-discharge measurements were performed, as shown in Figure 6. Figure 6a compares the CV curves of ZnO NRAs, ZnO/Mn₃O₄ NRAs and ZnO/Mn₃O₄ NTAs electrode collected in 0.5 M Na₂SO₄ at a scan rate of 5 mV/s. For ZnO/Mn₃O₄ core/shell nanostructures, the capacitive property only comes from Mn₃O₄ coating layers. Moreover, the pure ZnO nanorods almost no capacitive property is observed. In comparison with ZnO/Mn₃O₄ NRAs, ZnO/Mn₃O₄ NTAs exhibit higher capacitive current density and a nearly rectangular and symmetric CV shape, indicating the better electrochemical performance of ZnO/Mn₃O₄ NTAs than ZnO/Mn₃O₄ NRAs. Furthermore, all of the CV curves of ZnO/Mn₃O₄ NTAs at various scan rates show an almost-rectangular shape over the potential range in Figure 6b. For further evaluating the capacitive performance of ZnO/Mn₃O₄ NRAs and ZnO/Mn₃O₄ NTAs, galvanostatic charge-discharge testing was carried out. Figure 6c shows the charge-discharge curves of ZnO/Mn₃O₄ NRAs and ZnO/Mn₃O₄ NTAs at a current density of 3 A/g. Both their charge curves are relatively symmetric to their corresponding discharge curves, suggesting their good electrochemical behavior. Moreover, the discharge curve of ZnO/Mn₃O₄ NTAs is substantially prolonged over ZnO/Mn₃O₄ NRAs. The specific capacitance for the electrodes derived from galvanostatic charge-discharge can be calculated from the following equation:⁴⁰

$$C_{sp} = \frac{I \Delta t}{m \Delta V}$$

Where C_{sp} (F/g) is the specific capacitance, I (A) is the constant discharge current, dt (s) is the discharge time, dV (V) is the potential window, and m (g) is the mass of the active material in the working electrode (the active mass loading for ZnO/Mn₃O₄ NRAs and NTAs is about 0.23 and 0.27 mg/cm²). It is well known that a high C_{sp} value over a wide range of scan rates is very important for a electrode material practical application in supercapacitors. Galvanostatic charge-discharge curves at various current densities were also recorded to further evaluate the performance of the ZnO/Mn₃O₄ NTAs electrode, as shown in Figure 6d. Their charge curves are relatively symmetric to their corresponding discharge counterparts at the current densitied from 3 A/g to 24 A/g, further revealing the good capacitive behavior of the ZnO/Mn₃O₄ NTAs electrode. Figure 6e summarized the specific capacitance of the two electrodes calculated from their discharge curves with different scan rates. It is worth noting that the highest specific capacitance for ZnO/Mn₃O₄ NRAs and NTAs achieved 216.3 F/g and 441.4 F/g at the scan rate of 2 mV/s, respectively. Significantly, the specific capacitances for ZnO/Mn₃O₄ NTAs have 2-3 times higher than ZnO/Mn₃O₄ NRAs at scan rates between 2 and 100 mV/s. Such high specific capacitances of ZnO/Mn₃O₄ NRAs and NTAs can be mainly due to their unique structure. The uniform and ordered NRAs and NTAs can not only provide a fast electron transfer and a shorter ion diffusion pathway, but also facilitate the reaction of active species, and hence result in a good rate capability.

Because a long cycle life is among the most important criteria for a supercapacitor, an endurance test was conducted by using galvanostatic charging-discharging cycles

at a scan rate of 5 mV/s for 1000 cycles. The variation in the specific capacitance of ZnO/Mn₃O₄ NRAs and NTAs electrodes as a function of cycle number is shown in Figure 6f. There are only about 6.5% and 7.1% decreases in the specific capacitance of ZnO/Mn₃O₄ NRAs and NTAs after 1000 cycles, which indicates that ZnO/Mn₃O₄ NRAs and NTAs electrodes can withstand over 1000 cycles with no obvious decrease in the specific capacitance. These results are in contrast with experiments on other kinds of Mn₃O₄ electrodes, which showed significant degradation of the capacitance within the charging-discharging endurance tests.^{31, 41-42} Both the interior ZnO core and the exterior Mn₃O₄ motifs could make electrochemical contributions to the specific capacitance. Therefore, the ZnO/Mn₃O₄ NRAs and NTAs electrodes show high electrochemical stability for long-term capacitor applications.

The electrode kinetics of ZnO/Mn₃O₄ NRAs and NTAs were investigated by electrochemical impedance spectroscopy measurement (EIS) at room temperature, as shown in Figure 7. The Nyquist plots show a well-defined semicircle in the high-frequency region and a sloping line in the low-frequency region for the two samples. Such a pattern of the EIS can be fitted by an equivalent circuit shown in the inset of Figure 7, the diameter of the semicircle corresponds to the interfacial charge transfer (R_{ct}), which usually represents the resistance of the electrochemical reactions at the electrode surface,^{10, 31} and the sloping line is ascribed to the diffusion resistance of the electrolyte ion transfer in the electrode pores (Warburg impedance, W) and the proton diffusion in host materials.⁴³⁻⁴⁴ The calculated R_{ct} values accounting for the charge-transfer resistance are 16.8 Ω and 15.5 Ω for the ZnO/Mn₃O₄ NRAs and NTAs,

respectively. And the R_e values for ZnO/Mn₃O₄ NRAs and NTAs are 5.2 Ω and 5.0 Ω , respectively, which means that the electrodes have the different combination resistance of electrolyte, intrinsic resistance of active materials, and contact resistance at the active material/current collector interface. The most vertical line in the low-frequency region of the ZnO/Mn₃O₄ core/shell nanostructures indicates that ZnO/Mn₃O₄ NTAs possesses the better access path of electrolyte ions to the ZnO/Mn₃O₄ system. From the above analysis, it can be concluded that ZnO/Mn₃O₄ NTAs have a superior capacitive behavior, which is in consistent with the electrochemical measurement conducted above.

Conclusion

In summary, we have developed a simple electrodeposition approach to fabricate ideal supercapacitors based on the vertical and orderly 1D ZnO/Mn₃O₄ NRAs and NTAs electrodes. The ZnO/Mn₃O₄ NRAs and NTAs enable a fast and reversible redox reaction to improve the specific capacitance, especially for the ZnO/Mn₃O₄ NTAs which show superior electrochemical performance to ZnO/Mn₃O₄ NRAs such as high specific capacitance and good cyclic stability. These findings indicate that such 1D ZnO/Mn₃O₄ NTAs are very promising for next generation high-performance supercapacitors.

Acknowledgements

The authors acknowledge the financial support of this work by Natural Science Foundations of China (Grant No. 21306030), the Natural Science Foundations of

Guangdong Province (Grant No. s2012010009719 and s2013040015229), the Innovative Talents Cultivation Project of Guangdong Province (Grant No. LYM11096), the Science and Technology Project of Guangzhou (Grant No. 12C52011621 and 12C52011624), Scientific Research Project of Guangzhou Municipal Colleges and Universities (Grant No. 2012A064), and the Fresh Talent Program of Guangzhou University (Grant No. 201302).

References

- 1 P. Simon, Y. Gogotsi, *Nat. Mater.*, 2008, **7**, 845.
- 2 J. Feng, X. Sun, C. Wu, L. Peng, C. Lin, S. Hu, J. Yang, Y. Xie, *J. Am. Chem. Soc.*, 2011, **133**, 17832.
- 3 Q. Qu, S. Yang, X. Feng, *Adv. Mater.*, 2011, **23**, 5574.
- 4 X. Lu, D. Zheng, T. Zhai, Z. Liu, Y. Huang, S. Xie, Y. Tong, *Energy Environ. Sci.*, 2011, **4**, 2915.
- 5 M. F. El-Kady, V. Strong, S. Dubin, R. B. Kaner, *Science*, 2012, **335**, 1326.
- 6 Q. Li, Z. L. Wang, G. R. Li, R. Guo, L. X. Ding, and Y. X. Tong, *Nano Lett.*, 2012, **12**, 3803.
- 7 W. Yan, T. Ayvazian, J. Kim, Y. Liu, K. C. Donavan, W. Xing, Y. Yang, J. C. Hemminger, and R. M. Penner, *ACS Nano*, 2011, **5**, 8275.
- 8 S. Chen, J. Duan, Y. Tang, and S. Z. Qiao, *Chem. Eur. J.*, 2013, **19**, 7118.
- 9 G. Q. Zhang, H. B. Wu, H. E. Hoster, M. B. Chan-Park and X. W. Lou, *Energy Environ. Sci.*, 2012, **5**, 9453.

- 10 W. Yan, J. Kim, W. Xing, T. Ayvazian, and R. M. Penner, *Chem. Mater.*, 2012, **24**, 2382.
- 11 Y. B. He, G. R. Li, Z. L. Wang, C. Y. Su, Y. X. Tong, *Energy Environ. Sci.*, 2011, **4**, 1288.
- 12 L. Q. Mai, F. Yang, Y. L. Zhao, X. Xu, L. Xu, Y. Z. Luo, *Nat. Commun.*, 2011, **2**, 381.
- 13 G. R. Li, Z. L. Wang, F. L. Zheng, Y. N. Ou and Y. X. Tong, *J. Mater. Chem.*, 2011, **21**, 4217.
- 14 J. Liu, J. Jiang, C. Cheng, H. Li, J. Zhang, H. Gong, and H. J. Fan, *Adv. Mater.*, 2011, **23**, 2076.
- 15 L. Yu, G. Q. Zhang, C. Z. Yuan, X. W. Lou, *Chem. Commun.*, 2013, **49**, 137.
- 16 J. R. Miller, P. Simon, *Science*, 2008, **321**, 651.
- 17 M. D. Stoller, S. Park, Y. Zhu, J. An, R. S. Ruoff, *Nano Lett.*, 2008, **8**, 3498.
- 18 J. R. Miller, R. A. Outlaw, B. C. Holloway, *Science*, 2010, **329**, 1637.
- 19 X. Lang, A. Hirata, T. Fujita, M. Chen, *Nat. Nanotechnol.*, 2011, **6**, 232.
- 20 J. H. Kim, K. Zhu, Y. Yan, C. L. Perkins, A. J. Frank, *Nano Lett.*, 2010, **10**, 4099.
- 21 J. W. Lee, T. Ahn, J. H. Kim, J. M. Ko, J. D. Kim, *Electrochim. Acta*, 2011, **56**, 4849.
- 22 T. Y. Wei, C. H. Chen, K. H. Chang, S. Y. Lu, C. C. Hu, *Chem. Mater.*, 2009, **21**, 3228.

- 23 S. K. Meher, G. R. Rao, *J. Phys. Chem. C*, 2011, **115**, 15646.
- 24 Z. P. Feng, G. R. Li, J. H. Zhong, Z. L. Wang, Y. N. Ou, Y. X. Tong, *Electrochem. Commun.*, 2009, **11**, 706.
- 25 J. Zhang, J. Jiang, X. S. Zhao, *J. Phys. Chem. C*, 2011, **115**, 6448.
- 26 K.-H. Ye, Z.-Q. Liu, C.-W. Xu, N. Li, Y.-B. Chen, Y.-Z. Su, *Inorg. Chem. Commun.*, 2013, **30**, 1.
- 27 C. C. Hu, Y. T. Wu and K. H. Chang, *Chem. Mater.*, 2008, **20**, 2890.
- 28 W. Wei, X. Cui, W. Chen and D. G. Ivey, *Chem. Soc. Rev.*, 2011, **40**, 1697.
- 29 H. Jiang, T. Zhao, C. Yan, J. Ma and C. Li, *Nanoscale*, 2010, **2**, 2195.
- 30 M. Fang, X. Tan, M. Liu, S. Kang, X. Hu and L. Zhang, *CrystEngComm*, 2011, **13**, 4915.
- 31 X. Cui, F. Hu, W. Wei, W. Chen, *Carbon*, 2011, **49**, 1225.
- 32 C. L. Liu, K. H. Chang, C. C. Hu, W. C. Wen, *J. Power Sources*, 2012, **217**, 184.
- 33 K. Wang, X. Ma, Z. Zhang, M. Zheng, Z. Geng, and Z. Wang, *Chem. Eur. J.*, 2013, **19**, 7084.
- 34 L. Li, K. H. Seng, Z. Chen, H. Liu, I. P. Nevirkovets, Z. Guo, *Electrochim. Acta*, 2013, **87**, 801.
- 35 Z. Q. Liu, X. H. Xie, Q. Z. Xu, S. H. Guo, N. Li, Y. B. Chen, Y. Z. Su, *Electrochim. Acta*, 2013, **98**, 268.
- 36 D. Wang, Y. Li, Q. Wang, and T. Wang, *Eur. J. Inorg. Chem.*, 2012, 628.

- 37 J. Qu, F. Gao, Q. Zhou, Z. Wang, H. Hu, B. Li, W. Wan, X. Wang and J. Qiu, *Nanoscale*, 2013, **5**, 2999.
- 38 Z. Y. Tian, P. M. Kouotou, N. Bahlawane, and P. H. T. Ngamou, *J. Phys. Chem. C*, 2013, **117**, 6218.
- 39 Z. Q. Liu, K. Xiao, Q. Z. Xu, N. Li, Y. Z. Su, H. J. Wang, and S. Chen, *RSC Adv.*, 2013, **3**, 4372.
- 40 J. W. Lee, A. S. Hall, J. D. Kim, and T. E. Mallouk, *Chem. Mater.*, 2012, **24**, 1158.
- 41 G. An, P. Yu, M. Xiao, Z. Liu, Z. Miao, K. Ding and L. Mao, *Nanotechnology*, 2008, **19**, 275709.
- 42 Y. Wu, S. Liu, H. Wang, X. Wang, X. Zhang, G. Jin, *Electrochim. Acta*, 2013, **90**, 210.
- 43 M. W. Xu, W. Jia, S. J. Bao, Z. Su and B. Dong, *Electrochim. Acta*, 2010, **55**, 5117.
- 44 J. Ma, Q. Cheng, V. Pavlinek, P. Saha and C. Li, *New J. Chem.*, 2013, **37**, 722.

Figure Captions:

Figure 1. SEM images of (a-b) ZnO NRAs, (c-d) ZnO/Mn₃O₄ core/shell NRAs, and (e-f) ZnO/Mn₃O₄ core/shell NTAs.

Figure 2. XRD patterns of ZnO/Mn₃O₄ core/shell NRAs and NTAs.

Figure 3. (a-c) TEM and HRTEM image, (d) and the corresponding EDS pattern of ZnO/Mn₃O₄ core/shell nanorod obtained from an electrodeposition time of 15 min.

Figure 4. (a-b) TEM image, (c-f) HRTEM images and the corresponding SAED pattern of ZnO/Mn₃O₄ core/shell nanotube obtained from an electrodeposition time of 30 min, and (g-i) The corresponding EDX elemental mapping images of ZnO/Mn₃O₄ core/shell nanotubes.

Figure 5. XPS spectrum of ZnO/Mn₃O₄ core/shell NRAs and NTAs. (a) Binding energy spectrum of Zn 2p; (b) Binding energy spectrum of Mn 2p; (c) Binding energy spectrum of O 1s.

Figure 6. (a) CV curves of ZnO, ZnO/Mn₃O₄ core/shell NRAs and NTAs electrodes obtained at a scan rate of 5 mV s⁻¹; (b) CV curves of ZnO/Mn₃O₄ core/shell NTAs electrode at different scan rates; (c) Galvanostatic charge-discharge curves of ZnO/Mn₃O₄ core/shell NRAs and NTAs electrodes collected at a current density of 3 A g⁻¹; (d) Galvanostatic charge-discharge curves of ZnO/Mn₃O₄ core/shell NTAs electrode at different current density; (e) Plotted curves of the variation in the specific capacitance for ZnO/Mn₃O₄ core/shell NRAs and NTAs electrodes measured as a function of current density; (f) The variation of specific capacitance as a function of cycle number at 5 mV s⁻¹ for ZnO/Mn₃O₄ core/shell NRAs and NTAs.

Figure 7. Nyquist plots of ZnO/Mn₃O₄ core/shell NRAs and NTAs, the inset is the equivalent circuit.

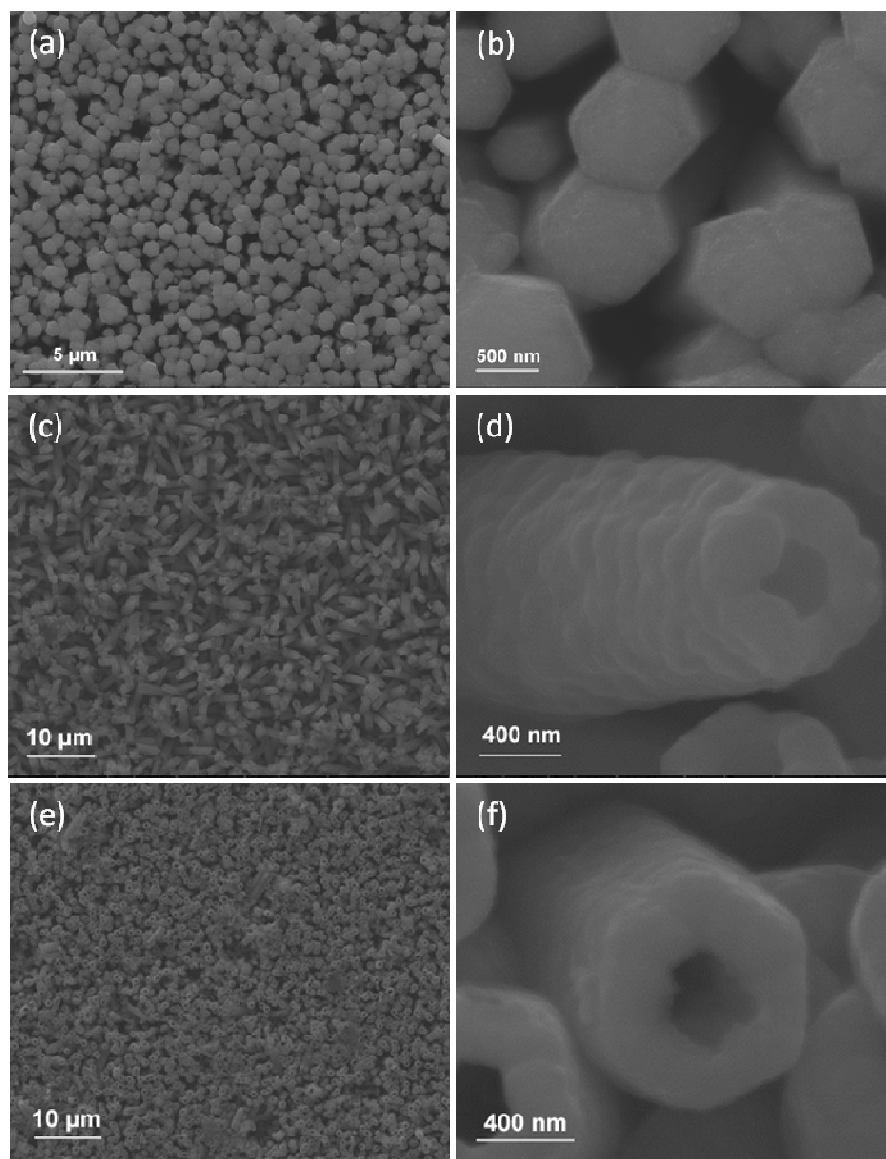


Figure 1.

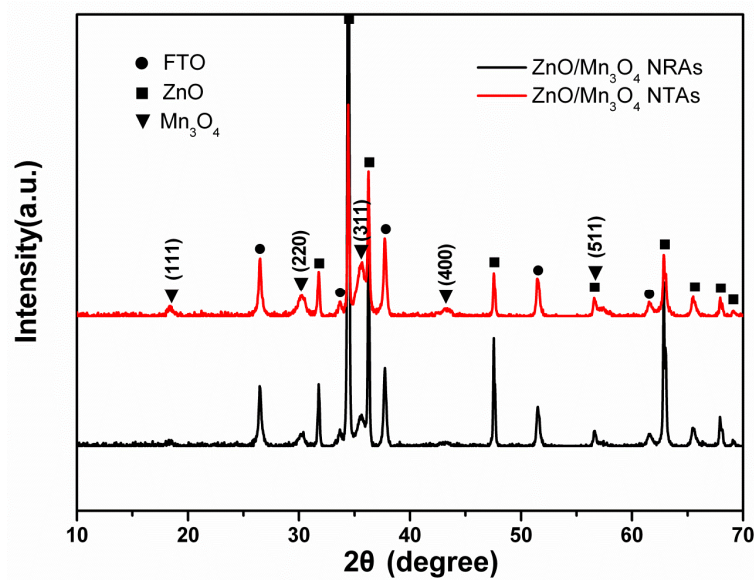


Figure 2.

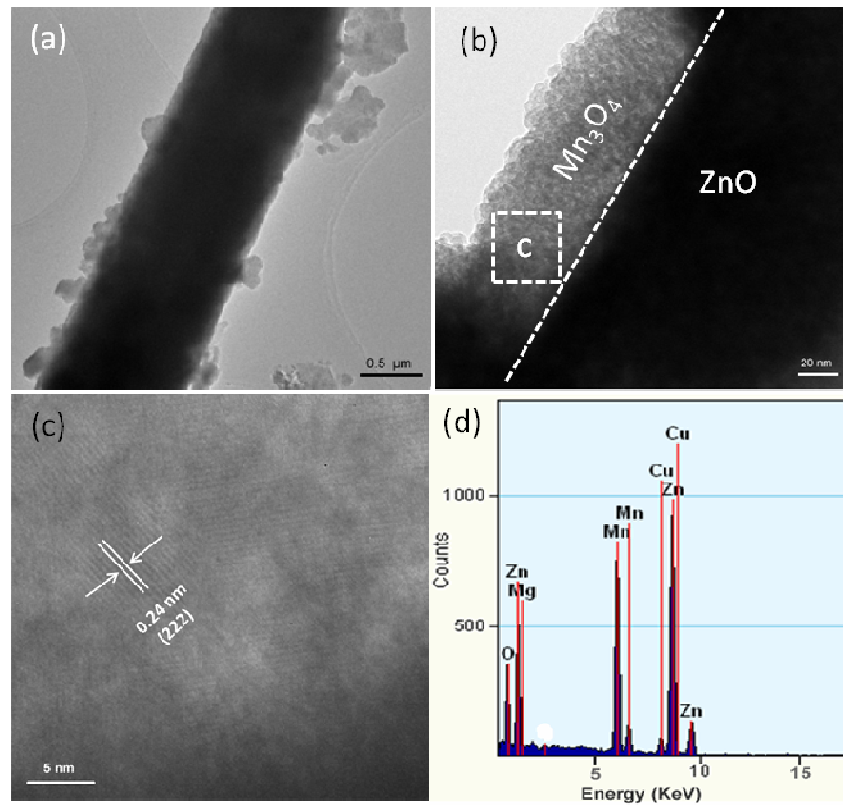


Figure 3.

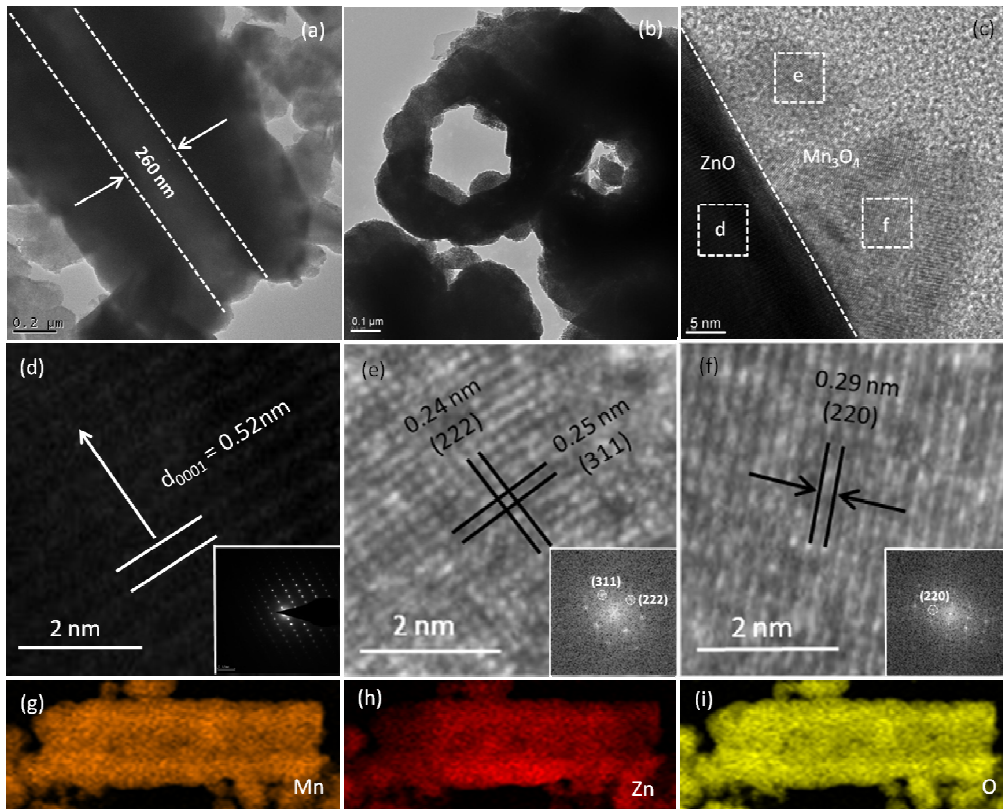


Figure 4.

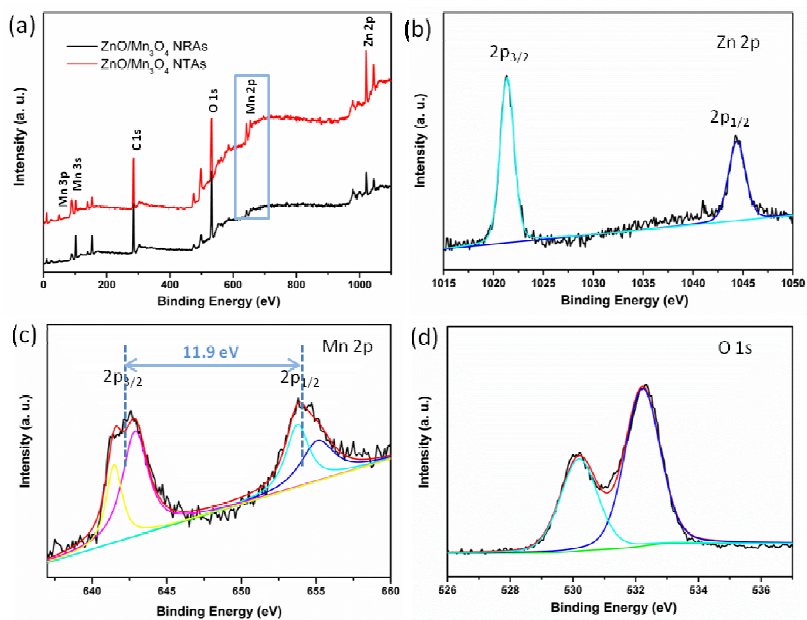


Figure 5.

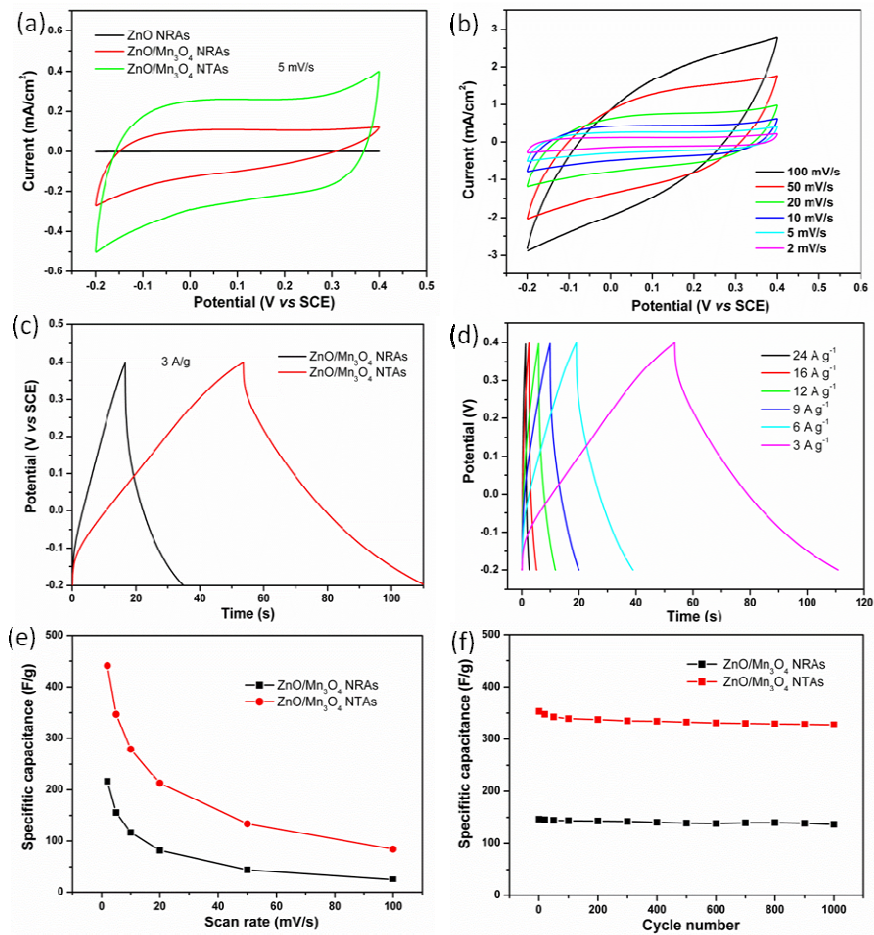


Figure 6.

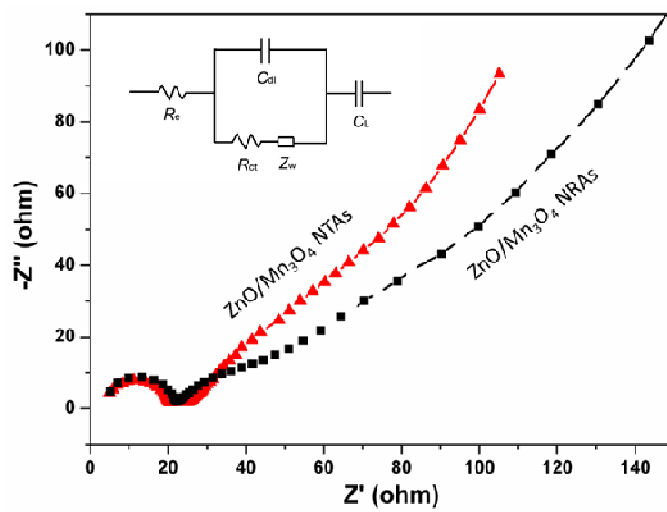


Figure 7.